Modelling Incomplete Solute Mixing at Pipe Junctions in Water Distribution Networks: Parametric CFD Simulations and a Predictive Regression Approach

Richárd Wéber[1], Levente Sándor[2], Gopinathan R. Abhijith[3], Sriman Pankaj Boindala[4], Avi Ostfeld[5]

[1] Department of Hydrodynamic Systems, Faculty of Mechanical Engineering, Budapest University of Technology and Economics, Műegyetem rkp. 3., H-1111 Budapest, Hungary; email: weber.richard@gpk.bme.hu, (Corresponding author)

[2] Department of Hydrodynamic Systems, Faculty of Mechanical Engineering, Budapest University of Technology and Economics, Műegyetem rkp. 3., H-1111 Budapest, Hungary; email: lsandor@hds.bme.hu

[3] Department of Civil Engineering, Indian Institute of Technology Kanpur, Kanpur 208016, UP, India; email: abhijith@iitk.ac.in

[4] Faculty of Civil and Environmental Engineering, Technion–Israel Institute of Technology, Haifa 32000, Israel; email: srimanpankaj@gmail.com

[5] Faculty of Civil and Environmental Engineering, Technion–Israel Institute of Technology, Haifa 32000, Israel; email: ostfeld@technion.ac.il

Highlights (max. 85 characters)

- CFD simulates the incomplete mixing in a four-way junction of distribution networks
- Five parameters are analysed with 864 parametric CFD simulations

- Regression fits a nonlinear function to predict the outflowing solute concentration
- Outlet concentration is mainly controlled by junction angle and inlet/outlet flow ratios.

Abstract

High-quality drinking water is essential for modern settlements, and accurate modelling of solute mixing at pipe junctions is crucial in water distribution networks (WDNs). While complete mixing is often assumed, recent studies emphasize the need to account for incomplete mixing. This paper advances the understanding of incomplete mixing effects on water quality dynamics in WDNs. Computational fluid dynamics (CFD) simulations are employed to examine how pipe connection angles in cross-junctions influence solute mixing. The results highlight the significance of the junction angle and the relative distribution of inflow and outflow rates, whereas the diffusion coefficient and the turbulent Schmidt number have a limited influence. A generic regression model is developed to capture the nonlinear relationships between the dominant factors, providing accurate predictions of mixing at pipe junctions with minimal computational cost. The model is validated against experimental data from the literature and can be integrated into traditional WDN solvers such as EPANET. The findings improve the simulation reliability of contaminant concentration profiles, supporting more robust water quality analysis and advancing the state of the art in WDN modelling.

Keywords (max. 6)

incomplete mixing, CFD, regression, OpenFOAM,

Introduction

Accurate modelling of solute mixing at pipe junctions is essential for predicting water quality in distribution systems (Shah and Sinai, 1988; Song et al., 2009). Traditional water quality models for water distribution systems (WDS) commonly assume that mixing at pipe junctions is complete and instantaneous (Fabrie et al., 2010; Ho, 2008; Pankaj et al., 2022). This assumption posits that when two or more streams of water meet, they merge entirely and form a homogeneous mixture immediately (Fabrie et al., 2010; Yousefian and Duchesne, 2022). While this simplification makes modelling more straightforward, it often fails to reflect real-world conditions (Ho, 2008; Yousefian et al., 2024). Experimental and computational studies have demonstrated that mixing is frequently incomplete (Grbčič et al., 2019; Hernández-Cervantes et al., 2018; Ho and Khalsa, 2009; Romero-Gomez et al., 2008; Song et al., 2009; Yu et al., 2014). The inaccuracies introduced by assuming complete mixing can lead to significant errors (Paez et al., 2017; Romero-Gomez et al., 2011) in water quality predictions, with outlet concentration errors sometimes reaching as high as 250% in scenarios of imperfect mixing (Yousefian and Duchesne, 2022).

The assumption of complete mixing at pipe junctions in WDSs oversimplifies the intricate dynamics of fluid interactions, leading to inaccuracies in water quality modelling. Variations in flow rates among converging streams significantly influence mixing efficiency; for instance, a dominant high-velocity stream can impede thorough solute distribution, resulting in concentration gradients (Cervantes et al., 2021; Ho and Khalsa, 2009). The geometry of pipe junctions—such as cross, T, and Y configurations—further complicates mixing behaviour, with each presenting unique challenges that affect how streams merge and interact (Romero-Gomez and Choi, 2011; Song et al., 2009). Additionally, the flow regime plays a crucial role: turbulent flows generally enhance mixing due to increased eddy diffusion, whereas laminar flows tend to limit mixing efficiency, leading to the stratification of solute concentrations (Yousefian et al., 2024). Overall, there is a clear need for studies to provide valuable insights into the dynamics of mixing and support the development of more realistic water quality models (Peng et al., 2024), incorporating scientifically sound theory and equations to simulate the mixing behaviour, especially at pipe junctions.

Several researchers have employed experimental and numerical methods to study solute mixing at pipe junctions. Experimental investigations involve physical setups designed to replicate various pipe-junction configurations. Tracers, such as salt or dye, are introduced to track fluid movement and mixing behaviour. Measurements of solute concentrations at different locations provide empirical data for evaluating mixing efficiency. Common junction types studied include cross-junctions, T-junctions, and Y-junctions, with variations in pipe diameters and flow rates used to simulate real-world conditions. While experimental studies yield accurate and reliable data, they are often time-consuming and resource-intensive (Austin et al., 2008; Shao et al., 2019; Song et al., 2018; Yousefian and Duchesne, 2024).

Numerical approaches, particularly computational fluid dynamics (CFD), offer a powerful alternative for analysing mixing at pipe junctions (Zhao et al., 2008). CFD simulations use mathematical models to describe fluid flow and solute transport, capturing the effects of advection, diffusion, and turbulence (Basha and Malaeb, 2007). These simulations provide detailed insights into the spatial and temporal evolution of mixing patterns (Grbčič et al., 2019; Romero-Gomez et al., 2008). However, CFD modelling can be computationally expensive, especially for large-scale water distribution networks. To address this challenge, researchers have focused on developing simplified surrogate models that incorporate the effects of incomplete mixing while maintaining computational efficiency (Ho and Khalsa, 2009; Yousefian et al., 2024; Yousefian and Duchesne, 2022).

Surrogate models, such as EPANET-BAM (Bulk Advective Mixing) (Ho and Khalsa, 2009), EPANET-IMX (Yousefian and Duchesne, 2024b), and AZRED (Song et al., 2009), were developed to offer practical alternatives to traditional assumptions by incorporating both physical and empirical insights. EPANET-BAM simulates mixing at pipe junctions based on the momentum of incoming flows, where streams with higher momentum dominate the outlet direction. This model employs a scaling parameter (with a default value of 0.5) for calibration and supports junctions with unequal pipe sizes through the BAM-WRAP extension. However, EPANET-BAM neglects diffusion and turbulent mixing, limiting its accuracy in many real-world scenarios where these effects are significant. It also performs poorly under laminar flow conditions (Yousefian and Duchesne, 2022). Despite these limitations, EPANET-BAM is readily available as an extension to the EPANET software.

EPANET-IMX is a recently developed surrogate model that simulates incomplete mixing at cross-junctions with large pipe diameters (Yousefian and Duchesne, 2022).

It has been calibrated and validated using experimental data and CFD simulations from a dedicated cross-junction setup. It offers a reliable and improved approach for modelling such scenarios as an EPANET extension. However, its applicability is constrained to cross-junctions, narrow flow ranges, and large-diameter pipes, limiting its ability to capture the full spectrum of real-world conditions.

AZRED, on the other hand, is an empirical model that predicts solute concentrations based on Reynolds number ratios using experimental data from various junction types (Song et al., 2009). While AZRED is validated for equal-diameter pipes and turbulent flow conditions, it does not account for laminar flows or junctions with unequal pipe diameters (Yousefian and Duchesne, 2022). Furthermore, its reliance on specific experimental conditions restricts its applicability to broader scenarios.

As summarized in Table 1, existing surrogate models represent a clear advancement beyond the complete mixing assumption; however, their applicability remains constrained. Most formulations demonstrate good performance under turbulent flow conditions and for fixed or well-defined geometries, but their accuracy becomes uncertain when applied to more complex hydraulic scenarios, such as varying junction geometries, unequal pipe configurations, or low Reynolds number flows. In particular, key physical aspects—such as geometric variability and transport-related effects—are often simplified or neglected. These limitations highlight the need for a more generalized and physically consistent formulation, which the present study addresses by systematically extending the parameter space to include both laminar and turbulent regimes, as well as geometric variations.

This article overcomes some of these limitations and proposes a regression model to capture incomplete mixing at junctions joining at different angles and under different flow regimes. This study presents comprehensive CFD simulations covering a wide range of parameters influencing mixing in a four-way junction. Turbulent and laminar cases are analysed for different angles, inlet and outlet ratios, diffusion coefficients, and turbulent Schmidt numbers, resulting in hundreds of cases. Regression models are fitted to achieve an efficient yet accurate approach for predicting outflow concentrations.

The paper is structured as follows. First, the CFD simulation setup is described in detail, introducing all considered scenarios. The regression analysis is then presented briefly, highlighting its key properties. The results section begins by validating the CFD results against experimental data from the literature and then presents the accuracy of the regression analysis. The discussion section addresses the primary limitations of the study and suggests directions for future work. Finally, the conclusion summarises the significance of the paper.

Materials and Methods

CFD Simulations

A symmetric four-way junction configuration was selected to investigate mixing properties, with two inlets and two outlets marked according to the cardinal directions, as shown in Figure 1. The two inlet patches supply water with and without a "virtual dye" using passive scalar transport to model solute mixing. The geometrical and physical parameter space is explored in a simple equidistant manner, shown in Table 2. For this investigation, *FreeCAD v1.0* is used for geometry preparation, *OpenFOAM v2313* for meshing and numerical simulations, and the *DAKOTA* framework to orchestrate these calculations with the pre- and post-processing tasks.

The junction consists of four branches with a 100 mm diameter and a length of ten diameters. The angle between the two symmetric branches is included as a geometrical parameter. An unstructured hexahedral mesh is created with three boundary layers and a refinement region in the mixing area to capture the flow features accurately, such as the boundary layer at the walls and mixing in the junction. The three-dimensional (3D) mesh is built using OpenFOAM's *snappyHexMesh* utility. A mesh-size dependency study is used to balance runtime efficiency and numerical accuracy. The optimal mesh size is determined to be 3 mm at the junction section (corresponding to approximately 20,000 overall cells), with a boundary-layer refinement of three prism layers with a first-layer height of 1.5 mm.

The simpleFoam solver ensures the validity of the incompressible Navier–Stokes equations, and an advection–diffusion equation is used to calculate solute spreading within the flow field. The standard *k*–*ε* turbulence model accounts for the effects of turbulence. Accurate and stable second-order numerical schemes are employed for the momentum, scalar, and turbulence equations. All calculations are run for 3,000 pseudo-time steps, during which all monitored quantities reach converged values and all residuals drop below 10^{-5}. Water is simulated using properties at 20 °C, with a kinematic viscosity of $10^{-6}\ \mathrm{m}^2/s$. Solute mixing is modelled as passive scalar transport, as the presence of the solute does not significantly influence the flow field. The solute diffusivity coefficient is varied between $10^{-8}$and $10^{-4}\ \mathrm{m}^2/s$. The turbulent Schmidt number governing mixing is defined using a prescribed turbulent mixing value in the *scalarTransport* utility.

The Reynolds number is defined using the Western pipeline, that is, with μ dynamic viscosity,

$$Re = \frac{v_W \rho D}{\mu} = \frac{4 Q_W \rho}{\pi D \mu} \quad (1)$$

where Re is the Reynolds number, Q_W is the flow rate in the Western inlet pipe, ρ is the density, D is the diameter and μ is the kinematic viscosity. The West boundary condition is defined as a volumetric flow-rate inlet corresponding to the prescribed Reynolds numbers, with a turbulence intensity of 5%. Similarly, the South patch is defined as an inlet, but the volumetric flow rate is multiplied by the inlet ratio to generate different mixing scenarios. The concentration at the West inlet is fixed to one, while that at the South inlet is fixed to zero. This approach reduces the number of independent parameters while preserving the general fluid-dynamical formulation of the problem. The outlets are defined as a volumetric flow-rate outlet at the East patch and a zero-pressure condition at the North boundary. The volumetric flow rate at the East patch is set by multiplying the sum of the inlet volumetric flow rates by an outlet ratio value. The parameters are listed in Table 2.

The parameter-space exploration study is carried out using the DAKOTA framework, which handles parameter definition, preprocessing, solver execution, and post-processing tasks for a total of 864 cases. The volumetric flow rate and scalar concentration are monitored at all outlets.

Regression model

A regression model can fit relationships between inputs and outputs without any connection to the physical phenomena by minimising the error between the CFD simulation and the regression model output. The question of interest in this case is the average outflow concentration at the Eastern outlet. The model of (Yousefian & Duchesne, 2024), originally formulated as a combination of flow-rate ratios, is extended by introducing multiplicative power-law terms dependent on the angle, the diffusion coefficient, and the turbulent Schmidt number.

$$C_E^* = \beta_1 \left(\log\left(\frac{Q_E}{Q_S}\right) + \beta_2 \left(\frac{Q_W}{Q_E}\right)^{\beta_3} \right) \alpha^{\beta_4} D^{\beta_5} Sc_t^{\beta_6} + \beta_7 \quad (2)$$

including the unknown β_i parameters. C_E^* is the normalised concentration at the Eastern pipeline. α is the angle of the junction, Sc_t is the turbulent Schmidt number and Q_E, Q_S and Q_w are the flow rate at the Eastern, Southern and Western branch respectively. The notations can be found in Table 2. The error is calculated using the least-squares method, i.e., the sum of the squares of the differences between the regression model and the CFD simulation. Since identification of the regression model parameters is nonlinear, the MATLAB built-in fitnlm function can overcome such an issue by utilising the Levenberg-Marquardt algorithm. With arbitrary input concentrations, the Eastern concentration can be rescaled

$$C_E = C_S + (C_W - C_S) C_E^* \quad (3)$$

and then the northern concentration is calculated as

$$C_N = \frac{Q_W C_W + Q_S C_S - Q_E C_E}{Q_N} \quad (4)$$

where C is the concentration and Q is the volumetric flow rate in different branches (E: Eastern, W: Western, S: Southern, N: northern).

Results

CFD simulations

A mesh independence study was performed to ensure that the selected mesh resolution provides sufficiently accurate results while keeping the parametric CFD campaign computationally feasible. A study is utilised with four different mesh sizes using an average scenario with a 60-degree angle, 1.0 inlet ratio, 0.4 outlet ratio, 10^{-5} diffusion coefficient and 0.1 turbulent Schmidt number. Figure 2 shows the findings of the study including the profile extraction locations, the velocity magnitudes, the turbulent kinetic energy and the concentration distribution. The final mesh parameters, such as the overall number of cells, the minimum cell size, and the boundary layer parameters, are finalised based on the mesh independence study.

The CFD model was validated against experimental data from (Yousefian & Duchesne, 2024) using corresponding turbulent cross-junction cases. Simulating scenarios with perpendicular junction, turbulent Reynolds number, 0.1 turbulent Schmidt number, and the corresponding inlet and outlet ratios results in 20 different cases, for which both simulation and measurement data are available. Figure 3 includes the results using a Bland-Altman plot. The validation variable is the Eastern concentration. The horizontal axis is the average of the simulation and the measurement, and the vertical axis is the difference between them. Ideally the black crosses align to zero horizontally, i.e., no difference. Figure 3 shows some overshoot on average, meaning that the CFD underpredicts the concentration. However, the agreement is within the experimental uncertainty reported in the reference study. Moreover, no systemic error is visible. The title of the plot presents the statistical data. The coefficient of determination is high, and the mean absolute error is low.

Figure 4 illustrates a midplane cut contour plot for the turbulent case with the inlet ratio being one and the outlet ratio being 0.4. In this scenario, the two well-developed flow branches converge in the junction area. After the two streams merge, they separate again asymmetrically due to the differing flow rate ratios at the outlets. As the angle increases, the two jets begin to work against each other, resulting in an unstable, more three-dimensional flow field characterised by secondary flows, as shown in Figure 4.

Mixing efficiency is highest at lower angles, where the jets join smoothly, with minimal interactions.

The branch lengths primarily affect (i) the degree to which inlet boundary conditions influence the junction flow and (ii) the extent to which outlet boundary conditions can feed back into the junction region. To mitigate these effects while keeping the computational campaign feasible, all four branches were set to a length of ten times the diameter. This provides sufficient development length upstream of the junction and a buffer downstream, so that the mixing dynamics in the junction are not dominated by the imposed boundary conditions. A branch length of ten pipe diameters is also consistent with previous recommendations by (Plesnaik & Cusano, 2005) and (Shao et al., 2014)

Regression analysis

Tables 2 and 3 present the numerical results of the regression model fitting for turbulent and laminar cases, respectively. The first column contains the index, the second is the parameter estimate, the third is the standard error, and the last is the p-value. The p-value shows the probability of the parameter being zero, i.e., having a statistically insignificant effect on the output. As Table 3 shows, in the case of turbulent flow, the influence of β_5 (the exponent of the diffusion coefficient) can be neglected. Although the p-value related to the turbulent Schmidt number suggests significant effect, the value of β_6 is still low. Since the turbulent Schmidt number typically cannot cover an extensive range, its overall effect can be neglected compared to the other parameters. The laminar case, see Table 4, highlights a similar effect, and both estimates for the influences of turbulent Schmidt number and the diffusion coefficient are low with high p values.

Figures 5 and 6 show the accuracy of the regression models compared to the CFD simulations. The first figure depicts the turbulent case with literature models (Shao et al., 2014; Yousefian & Duchesne, 2024) and the complete mixing model, while the latter is the laminar case. Both are visualised using Bland-Altman plots, i.e., the horizontal axis represents the average, and the vertical axis represents the difference between the regression model predictions and the CFD simulations for the Eastern concentration.

Figure 5 shows the X-Y scatter plots in the left panels and the Bland-Altman plots in the right panels for complete mixing, literature models (Yousefian & Duchesne, 2024, Shao et al., 2014) and the proposed model respectively in the case of turbulent flows. The inaccuracy of the complete mixing model is clear, as most points are located beneath the zero line highlighting significant offset error, meaning that the model overpredicts the outlet concentration. Moreover, the rest of the models do not show any systemic error and visually they have similar accuracy both regarding the offset and deviations. However, Figure 7 gives insight with statistical values. Even though (Yousefian & Duchesne, 2024) has the lowest MAE, the rest of the values show the superiority of the proposed method with highest R^2, the zero offset and the lowest standard deviation.

The title of Figure 6 contains the coefficients of determination (R^2) and the mean absolute errors (MAE) of the proposed model. The regression model predicts the laminar cases accurately, as indicated by the high coefficient of determination and low mean absolute error. The confidence interval, which is twice the standard deviation, is around 0.12, meaning the uncertainty remains low. Compared with the turbulent case, the laminar case shows a larger residual spread, although the overall agreement remains acceptable. A small number of cases show larger deviations, with residuals approaching -0.3.

Discussion

The results demonstrate a significant step forward in modelling incomplete mixing of solutes at pipe junctions within WDSs. While traditional process-based models, such as those implemented in the commonly used software like EPANET, rely on the assumption of complete and instantaneous mixing at the pipe junctions, the current study rigorously assessed the validity of this assumption by performing high-fidelity CFD simulations across an extensive range of hydraulic and geometric configurations.

The comprehensive parametric study, encompassing 864 simulation cases, explored the effects of junction angle, Reynolds number, inlet and outlet flow ratios, diffusion coefficient, and turbulent Schmidt number on the degree of mixing, quantified in terms of the normalized concentration at the Eastern outlet (C^*_E). As shown in Figure 8, C^*_E exhibits substantial variability across the tested parameter space, reaffirming that the assumption of complete mixing is invalid in most practical cases. Among all parameters, junction angle and inlet ratio demonstrated the strongest influence on outlet concentration, whereas Reynolds number, diffusion coefficient, and Schmidt number showed comparatively minor effects.

Nature of flow

In real-world WDSs, the flow in junctions is inherently three-dimensional and transient. However, to make the parametric study computationally feasible across hundreds of cases, the present work employed 3D, steady-state simulations. While this necessarily simplified the modelling framework, this enables a systematic exploration of mixing behaviour over a wide range of junction configurations.

Nonetheless, it is imperative to emphasise that although the flow is inherently transient, the essential physics of in-plane mixing can still be captured reasonably well with a steady-state model, especially for symmetric junctions. The results show that the simulations can capture key features of secondary flows, vortex formation, and concentration distribution in the mid-plane of the junction.

Some scenarios, particularly those with sharp angles or strong asymmetries in inlet momentum, exhibit unsteady behaviour suggestive of vortex shedding or edge-tone-like instabilities. These could be better resolved in transient simulations, but for most cases studied here, the steady-state assumption provided a sufficiently accurate representation of the mean flow and scalar transport patterns relevant for engineering design.

Characteristics of the cross-junction

The junction angle emerged as a minor influential factor affecting the mixing phenomenon among all the parameters explored. Therefore, it stands as the principal contribution of this work. The parametric extension over three angle configurations (60°, 90°, and 120°) offered valuable insights into how geometry governs the mixing behaviour.

Figure 4 illustrates how the pipe connecting angle impacts the interface between competing inlet jets and, consequently, the distribution of scalar concentrations at the outlets. The angle modifies the effective area available for mixing in two opposing ways. On one hand, increasing the angle beyond 90° increases the physical area over which the jets can interact. On the other hand, this also reduces the relative angle of attack between the competing flows from the West and South inlets, which in turn diminishes the shear and interaction intensity required for thorough mixing.

Figure 8 (top-left) also clearly shows that as the angle increases from 60° to 120°, the median C^*_E decreases, indicating weaker mixing at larger angles. The 60° configuration yields the broadest spread and highest median concentration at the eastern outlet, consistent with optimal interaction between the intersecting jets.

Altogether, the results show that mixing is most effective around the 60° configuration. Increasing the angle, either toward acute (e.g., 60°) or more obtuse (e.g., 120°) configurations, tends to decrease the degree of mixing. This is evident in both the scalar concentration profiles and in the error metrics of the surrogate model, as the accuracy of the regression is the lowest with extreme-angle cases.

Role of inlet ratio

The inlet flow ratio governed the relative momentum of competing jets entering the junction, thereby directly influencing the mixing interface position. Figure 8 (middle-left) shows a clear declining trend in C^*_E with increasing inlet ratio. When the flow from one inlet dominates, the jet shifts the mixing interface toward the weaker stream, skewing the scalar distribution accordingly. Though the effect is relatively less pronounced compared to that of the junction angle, variations in inlet flow ratio can lead to outlet concentration differences exceeding 15-20% compared to the equal-inlet-flow baseline. This sensitivity underscored the importance of incorporating the inlet flow ratio as a parameter in the surrogate model of mixing at cross-junctions, especially under transient conditions when the flow separations occur dynamically.

Role of outlet ratio

Like the inlet ratio, the outlet ratio influences how the fluid parcels are extracted from the junction. This is evident from Figure 8 (middle-right). A higher outlet flow rate could favour movement of the fluid toward that direction, effectively stretching and shifting the scalar plume in that direction. Our analysis indicates that outlet flow separation has a non–negligible effect on scalar distribution. In particular under laminar flow conditions, differences in outlet ratios caused changes in outlet concentrations of up to 10–12%. Although this is less critical than inlet conditions or junction angle, accurate representation of the outlet ratios is found necessary for predictive modelling, especially under highly dynamic operating conditions.

Influence of diffusion

It is difficult to generalize the influence of diffusion due to its dependence on the physicochemical properties of the transported solute (e.g., molecular diffusivity), as well as temperature, pipe material, and other environmental factors. The typical range of diffusion coefficients of solutes in water distribution networks is from 10^{-7} to 10^{-9} m^2/s (Mottahedin et al., 2024; Schramke et al., 1999). To address this variability, we performed simulations at the top range of diffusion coefficient and even beyond to assess whether any effect is present. As shown in Figure 8 (bottom-left), changes in C^*_E across these values are minimal, confirming that molecular diffusion plays an insignificant role in determining mixing at the scales relevant to WDS junctions.

The Peclet number (Pe), defined as the product of Reynolds (Re) and Schmidt (Sc) numbers, provides a convenient nondimensional estimate of the relative strength of advective to diffusive transport. In most real-world cases, where Re > 10^4 and Sc between 0.1 and 1, Pe remains large, indicating that advection governs the transport process. Our CFD simulations supports this conclusion (Figure 8, bottom-right), with changes in Sc over an order of magnitude leading to only marginal changes in outlet concentration profiles (typically below 5%). This further justifies the emphasis on advective mechanisms, particularly the role of jet interaction and junction geometry, in shaping scalar transport behaviour.

Applications of the generic model

The generic power-law regression model used in this study is a product-form extension of the analytical framework proposed by Yousefian and Duchesne (2024). The model incorporates parameters such as junction angle, inlet and outlet ratios, Re, and Sc. The model is capable of predicting water quality (solute concentration) at the outlets of cross-junctions with high accuracy. In turbulent regimes, the proposed model achieved an R^2 value of 0.86 and an MAE of ~0.05. This proves the ability of the surrogate model to capture the complex mixing phenomena.

While the results corresponding to turbulent flow regimes are highly encouraging, the performance in the laminar regime is more variable, particularly for extreme geometries such as the 60° junction case, as shown in Figure 9.

The velocity and concentration fields in the midplane reveal two sharply defined jets entering the junction, leading to strong competition and a highly unstable flow structure within the elbow region (Figure 9). This behaviour highlights a key limitation of the present modelling framework: while the steady-state simulations provide meaningful insights into in-plane mixing behaviour, they do not capture transient effects, which are particularly relevant in low-Re, geometrically complex scenarios. Compared to the turbulent flow regime, although the performance of the model in the laminar regime is comparatively lower, it can still be deemed acceptable given the increased variability and inherent sensitivity of laminar flows to boundary conditions and geometry-induced instabilities. Extending the analysis to time-dependent simulations could provide greater fidelity in laminar flow conditions. However, the computational expense associated with transient simulations, especially when applied to a high-dimensional parameter space, is prohibitive. A single transient 3D simulation could take two to three orders of magnitude more computational time than its steady counterpart, thereby limiting the feasibility of such an approach for large-scale surrogate model generation.

Although the proposed surrogate model is physically interpretable and mathematically convenient, it holds the limitation that it is not rigorously derived from fundamental fluid dynamics equations. Rather, it is guided by engineering insight, dimensional analysis, and the empirical nature of the derived dataset. This approach offers the advantage of transparency and ease of integration into traditional network solvers, but it may limit the model's capacity to capture complex nonlinearities or flow separations that do not conform to the assumed structure. Alternative modelling techniques, such as deep learning, could potentially overcome this limitation by learning arbitrary functional forms directly from the data. However, such models often lack interpretability and are challenging to integrate into solvers like EPANET, which depend on explicit algebraic formulations of nodal mixing behaviour.

Nevertheless, the dimensionless formulation, incorporating Re, Sc, junction angle, and flow ratios, is a stronghold of the proposed surrogate model. This could enable the extrapolation of the model to a broad range of physical conditions existing in WDS beyond the specific ranges simulated in this study. The path forward involves the integration of the surrogate model into water quality solvers, either through external coupling or by embedding it directly into their codebases. Such a development would enable more accurate simulation of solute transport in WDS while retaining computational efficiency and compatibility with existing planning and operational tools. Ultimately, this integration would contribute to the development of a new generation of open-source and computationally efficient software platforms for water quality modelling, thereby enhancing the reliability of predictions and supporting informed decision-making for infrastructure management.

Complete mixing versus incomplete mixing

The quantitative differences between the ideal mixing assumption and the CFD-based results obtained are significant. In turbulent flows with a Re of 10,000 and a junction angle of 90°, outlet concentrations deviated by 18–22% from those predicted by the complete mixing model when inlet flow ratios are asymmetric. In laminar flows at a Re of 1,000, deviations exceeded 35%, particularly when the angle between inlets created elongated interaction zones or pronounced flow separation. These discrepancies are of particular concern in contaminant transport modelling, real-time water quality monitoring, and sensor placement strategies, where the 'misjudgements' in nodal mixing predictions can propagate through the distribution network and yield erroneous conclusions that increase the risks of failures. The results clearly demonstrated that accounting for incomplete mixing at junctions is not merely a theoretical improvement, but a necessary modification to increase the accuracy, reliability, and as well as the practicality of water quality models for WDSs.

Conceptual framework

The proposed incomplete-mixing equation can be incorporated into conventional process-based water-quality models by replacing the complete-mixing calculation at network junctions. Such models use the hydraulic model outputs, such as flow velocity and flow rates in pipes, pressures and outflows at every node, inflows and outflows along with water levels in tanks, status of pumps and valves, etc., as inputs to begin with. Since the spatiotemporal dynamics of water quality in distribution pipes are governed by both transport and reactions, advective-reactive partial differential equations are typically used to describe the behaviour of contaminants in these pipes. Such equations lack closed-form solutions for the dynamic initial and boundary conditions we encounter in WDN operations. Hence, numerical approaches are typically employed to solve them. An Eulerian-based numerical approach for solving the advective-reactive partial differential equations is described in the following paragraph. The details of the modelling framework are graphically represented in Figure 10.

The first step involves discretising the temporal domain into discrete time steps. For every timestamp, the WDNs, specifically the pipes, must be discretised spatially into grid points with a spatial resolution. This discretisation is based on the Courant-Friedrichs-Lewy (CFL) condition and is governed by the flow velocity in the pipe at the time step of interest. Once the spatial and temporal discretisation is established, the advective-reactive partial differential equations governing contaminant transport in each pipe is solved numerically. The solution process essentially captures the downstream transport of contaminants driven by flow (advection) and their simultaneous transformation due to physical, chemical, or biological processes (reactions).

At each time step, the concentration profile along a pipe is advanced by accounting for the movement of water parcels from upstream to downstream segments, based on the flow velocity obtained from the hydraulic model. Superimposed on this transport is the effect of reactions, such as decay of disinfectants or formation of by-products, which are incorporated as source or sink terms within each segment. Boundary conditions play a crucial role in this step, as the concentration entering a pipe from its upstream node (or tank/reservoir) determines how the contaminant plume evolves within the pipe. By repeating this process across all pipes in the network, a consistent update of concentrations throughout the distribution network is obtained for the given time step.

After updating the concentrations within the pipes, the model computes concentrations at the nodes (Figure 10). This is typically done under the assumption of complete and instantaneous mixing. In practical terms, this means that all water entering a node from multiple connecting pipes is assumed to mix perfectly before leaving the node. This is where the proposed equations come into play. Rather than assuming complete mixing, the proposed equations provide a more realistic representation of concentration distributions at nodes by accounting for partial mixing (Figure 10). The empirical equation is readily integrable into the existing numerical framework and serves as a computationally efficient substitute for the complete mixing assumption, thereby improving the fidelity of water-quality predictions without significantly increasing model complexity. The nodal concentrations thus serve as updated boundary conditions for the connected downstream pipes in the subsequent time step.

In this manner, the solution of the advective-reactive equation within pipes, combined with the in-complete mixing assumptions at nodes, enables a stepwise propagation of water quality throughout the network.

Conclusion

The paper presents a general modelling approach to describe incomplete solute mixing in water distribution network junctions using computational fluid dynamics. Simulations conducted in the *DAKOTA* environment cover 864 cases, varying parameters such as junction angle, inflow and outflow ratios, turbulent Schmidt number, and diffusion coefficients for both turbulent and laminar flows. *OpenFOAM* ensures the accurate solution of the fluid dynamical equations. The CFD model is validated against measurement data from the literature for the perpendicular junction case, while mesh independence study ensures numerical reliability. Nonlinear regression analysis fits a closed-form function to predict the outflowing solute concentration based on the input parameters and also highlights the negligible effect of the turbulent Schmidt number and the diffusion coefficients, and the importance of in- and outflow ratios and the angle of the junction. The proposed method is compared with literature models under turbulent flow conditions and demonstrates superior performance, with lower standard deviation and zero offset error. In addition to turbulent flow, the paper also presents a regression model for laminar flow conditions. Despite strong agreement between the regression model and simulation data, as demonstrated by *Bland-Altman* plots, coefficient of determination, and mean absolute error, some outliers remain due to unmodeled 3D and transient effects. The proposed regression model can be easily integrated into traditional network solvers like EPANET, offering a practical tool for improving solute transport predictions in water distribution systems.

Acknowledgement

This research was supported by the Israeli Water Authority under project number 143990. Project no. TKP-6-6/PALY-2021 has been implemented with the support provided by the Ministry of Culture and Innovation of Hungary from the National Research, Development and Innovation Fund, financed under the TKP2021-NVA funding scheme.

Data Availability Statement

Some or all data, models, or code that support the findings of this study are available from the corresponding author upon reasonable request.

Supplemental Materials

Additional details of the CFD simulation setup, meshing procedure and solver configuration are provided in the Supplemental Materials, see https://doi.org/10.5281/zenodo.18493465

References

Austin, R.G., Waanders, B. van B., McKenna, S., Choi, C.Y., 2008. Mixing at Cross Junctions in Water Distribution Systems. II: Experimental Study. J Water Resour Plan Manag 134, 295–302. https://doi.org/10.1061/(ASCE)0733-9496(2008)134:3(295)

Basha, H. A., and Malaeb, L. N. (2007). “Eulerian–Lagrangian method for constituent transport in water distribution networks.” *Journal of Hydraulic Engineering*, **133**(10), 1155–1166. https://doi.org/10.1061/(ASCE)0733-9429(2007)133:10(1155)

Cervantes, D.H., Amparo López-Jiménez, P., Nevárez, J.A.A., Galván, X.D., Magaña, M.R.J., Pérez-Sánchez, M., De Jesús Mora Rodríguez, J., 2021. Incomplete mixing model at cross-junctions in epanet by polynomial equations. Water (Switzerland) 13. https://doi.org/10.3390/W13040453

Fabrie, P., Gancel, G., Mortazavi, I., and Piller, O. (2010). “Quality modeling of water distribution systems using sensitivity equations.” Journal of Hydraulic

Engineering, 136(1), 34–44. https://doi.org/10.1061/(ASCE)HY.1943-7900.0000138

Grbčič, L., Kranjčević, L., Lučin, I., Čarija, Z., 2019. Experimental and numerical investigation of mixing phenomena in double-Tee junctions. Water (Switzerland) 11. https://doi.org/10.3390/W11061198

Hernández-Cervantes, D., Delgado-Galván, X., Nava, J.L., López-Jiménez, P.A., Rosales, M., Rodríguez, J.M., 2018. Validation of a computational fluid dynamics model for a novel residence time distribution analysis in mixing at cross-junctions. Water (Switzerland) 10. https://doi.org/10.3390/W10060733

Ho, C. K. (2008). "Solute mixing models for water-distribution pipe networks." Journal of Hydraulic Engineering, 134(9), 1236–1244. https://doi.org/10.1061/(ASCE)0733-9429(2008)134:9(1236)

Ho, C.K., Khalsa, S.S., 2009. Epanet-BAM: Water quality modeling with incomplete mixing in pipe junctions. Proceedings of the 10th Annual Water Distribution Systems Analysis Conference, WDSA 2008 981–991. https://doi.org/10.1061/41024(340)87

Mottahedin, A., Giudicianni, C., Di Nunno, F., Granata, F., Cunha, M., Walski, T., & Creaco, E. (2024). Analysis, design, and maintenance of isolation valves in water distribution networks: State of the art review, insights from field experiences and future directions. In *Water Research* (Vol. 262). Elsevier Ltd. https://doi.org/10.1016/j.watres.2024.122088

Paez, N., Saldarriaga, J., Bohorquez, J., 2017. Water Quality Modeling Considering Incomplete Mixing in Extended Periods. Procedia Eng 186, 54–60. https://doi.org/10.1016/j.proeng.2017.03.207

Pankaj, B.S., Jaykrishnan, G., Ostfeld, A., 2022. Optimizing Water Quality Treatment Levels for Water Distribution Systems under Mixing Uncertainty at Junctions. J Water Resour Plan Manag 148, 4022013. https://doi.org/10.1061/(ASCE)WR.1943-5452.0001544

Peng, Z., Stovin, V., and Guymer, I. (2024). "Radial mixing in steady and accelerating pipe flows." *Journal of Hydraulic Engineering*, **150**(6), 04024047. https://doi.org/10.1061/JHEND8.HYENG-14071

Plesniak, M., Cusano, D., 2005. Scalar mixing in a confined rectangular jet in crossflow. J. Fluid Mech. 524, 1-45. https://doi.org/10.1017/S0022112004001132

Romero-Gomez, P., Choi, C.Y., 2011. Axial Dispersion Coefficients in Laminar Flows of Water-Distribution Systems. Journal of Hydraulic Engineering 137, 1500–1508. https://doi.org/10.1061/(ASCE)HY.1943-7900.0000432

Romero-Gomez, P., Ho, C.K., Choi, C.Y., 2008. Mixing at Cross Junctions in Water Distribution Systems. I: Numerical Study. J Water Resour Plan Manag 134, 285–294. https://doi.org/10.1061/(ASCE)0733-9496(2008)134:3(285)

Romero-Gomez, P., Lansey, K.E., Choi, C.Y., 2011. Impact of an incomplete solute mixing model on sensor network design. Journal of Hydroinformatics 13, 642–651. https://doi.org/10.2166/HYDRO.2010.123

Schramke, J. A., Murphy, S. F., Doucette, W. J., & H, W. D. (1999). PREDICTION OF AQUEOUS DIFFUSION COEFFICIENTS FOR ORGANIC COMPOUNDS AT 25°C. In *Chemosphere* (Vol. 38, Issue 10).

Shah, M., and Sinai, G. (1988). “Steady state model for dilution in water networks.” *Journal of Hydraulic Engineering*, **114**(2), 192–206. https://doi.org/10.1061/(ASCE)0733-9429(1988)114:2(192)

Shao, Y., Jeffrey Yang, Y., Jiang, L., Yu, T., & Shen, C. (2014). Experimental testing and modeling analysis of solute mixing at water distribution pipe junctions. Water Research, 56, 133–147. https://doi.org/10.1016/j.watres.2014.02.053

Shao, Y., Zhao, L., Yang, Y.J., Zhang, T., Ye, M., 2019. Experimentally Determined Solute Mixing under Laminar and Transitional Flows at Junctions in Water Distribution Systems. Advances in Civil Engineering 2019. https://doi.org/10.1155/2019/3686510

Song, I., Romero-Gomez, P., Andrade, M.A., Mondaca, M., Choi, C.Y., 2018. Mixing at junctions in water distribution systems: an experimental study. Urban Water J 15, 32–38. https://doi.org/10.1080/1573062X.2017.1364395

Song, I., Romero-Gomez, P., Choi, C.Y., 2009. Experimental Verification of Incomplete Solute Mixing in a Pressurized Pipe Network with Multiple Cross Junctions. Journal of Hydraulic Engineering 135, 1005–1011. https://doi.org/10.1061/(ASCE)HY.1943-7900.0000095

Yousefian, R., Duchesne, S., 2024. Experimental study of mixing phenomenon in water distribution networks under real-world conditions. https://doi.org/10.4995/WDSA-CCWI2022.2022.14040

Yousefian, R., Duchesne, S., 2022. Modeling the Mixing Phenomenon in Water Distribution Networks: A State-of-the-Art Review. J Water Resour Plan Manag 148, 3121002. https://doi.org/10.1061/(ASCE)WR.1943-5452.0001513

Yousefian, R., Duchesne, S., Schwarz, P.-O., 2024. Investigating incomplete mixing models in cross junctions under real-world conditions of water distribution networks. Water Supply 24, 3148–3160. https://doi.org/10.2166/WS.2024.187

Yousefian, R., & Duchesne, S. (2024). Improving incomplete mixing modeling for junctions of water distribution networks. Journal of Hydroinformatics. https://doi.org/10.2166/hydro.2024.041

Yu, T.C., Shao, Y., Shen, C., 2014. Mixing at Cross Joints with Different Pipe Sizes in Water Distribution Systems. J Water Resour Plan Manag 140, 658–665. https://doi.org/10.1061/(ASCE)WR.1943-5452.0000372

Zhao, C.-H., Zhu, D. Z., and Rajaratnam, N. (2008). "Computational and experimental study of surcharged flow at a 90° combining sewer junction." *Journal of Hydraulic Engineering*, **134**(6), 688–700. https://doi.org/10.1061/(ASCE)0733-9429(2008)134:6(688)

Figure Caption List

Figure 1. Junction geometry with parameters and noting Western, Eastern, Southern and Northern pipelines with flow directions.

Figure 2. The top-left plot shows the mesh structure for the 200k-cell mesh and the locations of the profile extraction along both the x- and y-axes. The centre and bottom-left panels show the velocity magnitude and turbulent kinetic energy profiles along the centrelines of the west and east pipes. The right-side panels show the concentration, velocity magnitude, and turbulent kinetic energy profiles extracted near the inlet of the junction region.

Figure 3. Bland-Altman plot is used to validate CFD simulations based on the Eastern concentration.

Figure 4. Midplane cut of the velocity and concentration fields for a turbulent case with a 0.4 outlet ratio at a) 60 degrees, b) 90 degrees, and c) 120 degrees angles.

Figure 5. Bland-Altman diagram of CFD results and prediction by regression model. The solid red line depicts the average, while the dashed red lines are twice the average ± twice the standard deviation. The title contains the coefficient of determination (R^2) and mean absolute error (MAE) in the case of turbulent flow (Re=10000).

Figure 6. Bland-Altman diagram of CFD results and prediction by regression model. The solid red line depicts the average, while the dashed red lines are twice the average ± twice the standard deviation. The title contains the coefficient of determination (R^2) and mean absolute error (MAE) in the case of laminar flow (Re=1000).

Figure 7. Bar charts illustrate the accuracy of the complete mixing and incomplete mixing models using four statistical metrics. The bar corresponding to the complete mixing model (Complete*) is truncated, as its actual value (−2.638) would otherwise distort the scale of the plot without providing additional insight.

Figure 8. Boxplots indicating the effect of the parametric study to the Eastern concentration.

Figure 9. Midplane cut of the velocity and concentration fields for the worst agreement on the laminar case with 60° angle geometry.

Figure 10. Framework for process-based water quality predictive modelling for WDNs. (A) represents the complete mixing assumption and (B) represents the incomplete mixing assumption.

Tables

Table 1: Comparison of incomplete mixing models for cross junctions

Feature	This study	Yousefian & Duchesne (2024)	Shao et al. (2014)
Junction type	Cross junction	Cross junction	Cross junction & Double-tee
Geometry variation (angle)	Included (60°, 90°, 120°)	Not considered	Not considered
Flow regimes	Laminar + turbulent	Turbulent	Turbulent
Number of cases	864 CFD	25 experiments + CFD	23 experiments + CFD
Parameter space	Multi-dimensional (Re, angle, inlet/outlet ratios, diffusion)	Flow ratios + pipe size configurations	Flow ratios + geometry
Diffusion effects	Explicitly analysed (10^{-8}–10^{-4} m^2/s)	Not considered	Not considered
Turbulent Schmidt number	Explicitly analysed	Implicit via CFD calibration	Not considered
Model type	Regression (generalised, multi-parameter)	Regression equation	Semi-empirical / analytical

Table 2: The explored parameter space with a total combination of 864. Figure 1 indicates the positioning of Western (W), Southern (S) and Eastern (E) pipelines. Re is the Reynolds number of the Western pipeline.

Notation	**Name**	Unit	Parameters			
α	**Angle**	[deg]	60	90	120	
Re	**Reynolds number**	[-]	1000	10000		
$\mathrm{Q_S/Q_W}$	**Inlet ratio**	[-]	0.5	1.0	1.5	2.0
$\mathrm{Q_E/(Q_S+Q_W)}$	**Outlet ratio**	[-]	0.2	0.4	0.6	0.8
D	**Diffusivity coefficient**	[m2/s]	1.00E-04	1.00E-05	1.00E-08	
$\mathrm{Sc_t}$	**Turbulent Schmidt number**	[-]	1.00	0.10	0.01	

Table 3 Fitted β_i parameters of the regression model for turbulent flow ($Re = 10000$) with the standard error, and the p value showing the probability of the parameter being equal to zero.

	$\boldsymbol{\beta_i}$	**standard error**	**p-value**
1	0.1188	0.0218	<0.001
2	4.511	0.434	<0.001
3	1.146	0.0704	<0.001
4	-0.1645	0.0346	<0.001
5	0.001604	0.00246	0.5149
6	-0.02908	0.00534	<0.001
7	-0.114	0.0195	<0.001

Table 4 Fitted β_i parameters of the regression model for laminar flow ($Re = 1000$) with the standard error, and the p value showing the probability of the parameter being equal to zero

	$\boldsymbol{\beta_i}$	**standard error**	**p-value**
1	0.2790	0.0415	<0.001
2	4.217	0.372	<0.001
3	0.798	0.0707	<0.001
4	-0.2106	0.0329	<0.001
5	0.004857	0.00212	0.0223
6	-0.00514	0.00431	0.2332
7	-0.2398	0.0411	<0.001

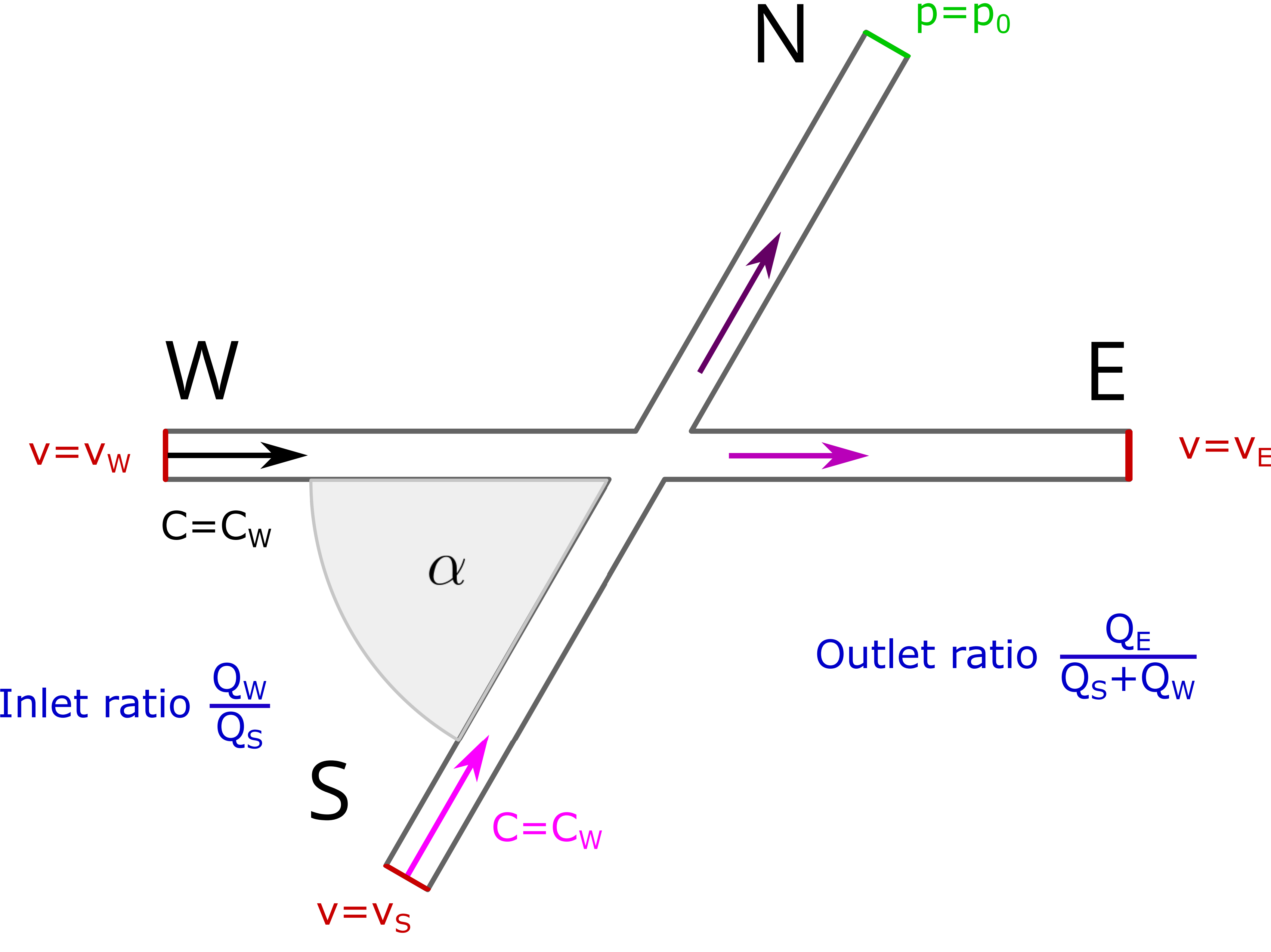
N
p=p0
W
E
v=vW
v=vE
C=CW
α
Outlet ratio QE / QS+QW
Inlet ratio QW / QS
S
C=CW
v=vS

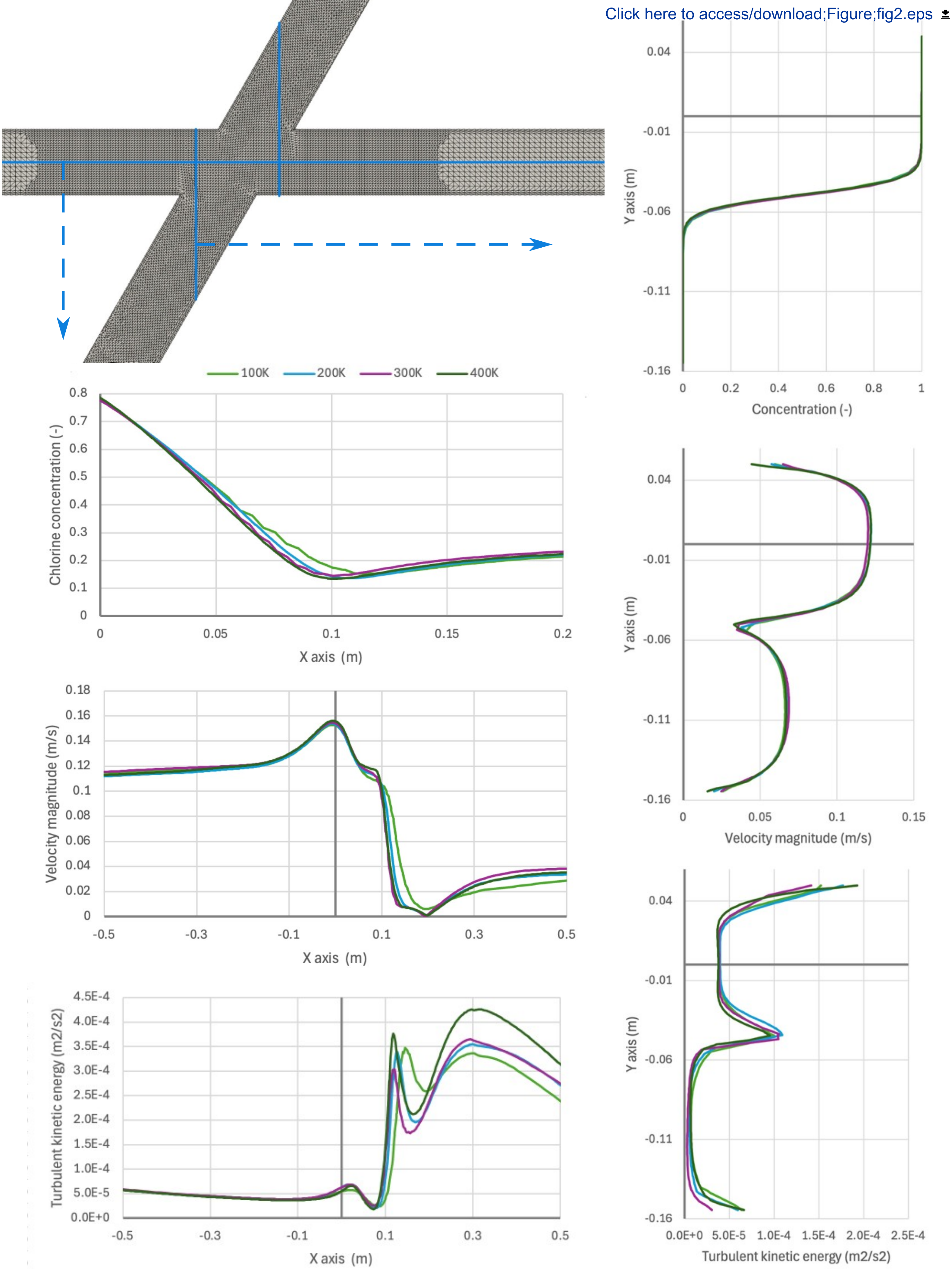

100K
200K
300K
400K
Concentration (-)
Y axis (m)
Chlorine concentration (-)
X axis (m)
Velocity magnitude (m/s)
Y axis (m)
X axis (m)
Velocity magnitude (m/s)
Turbulent kinetic energy (m2/s2)
X axis (m)
Y axis (m)
Turbulent kinetic energy (m2/s2)

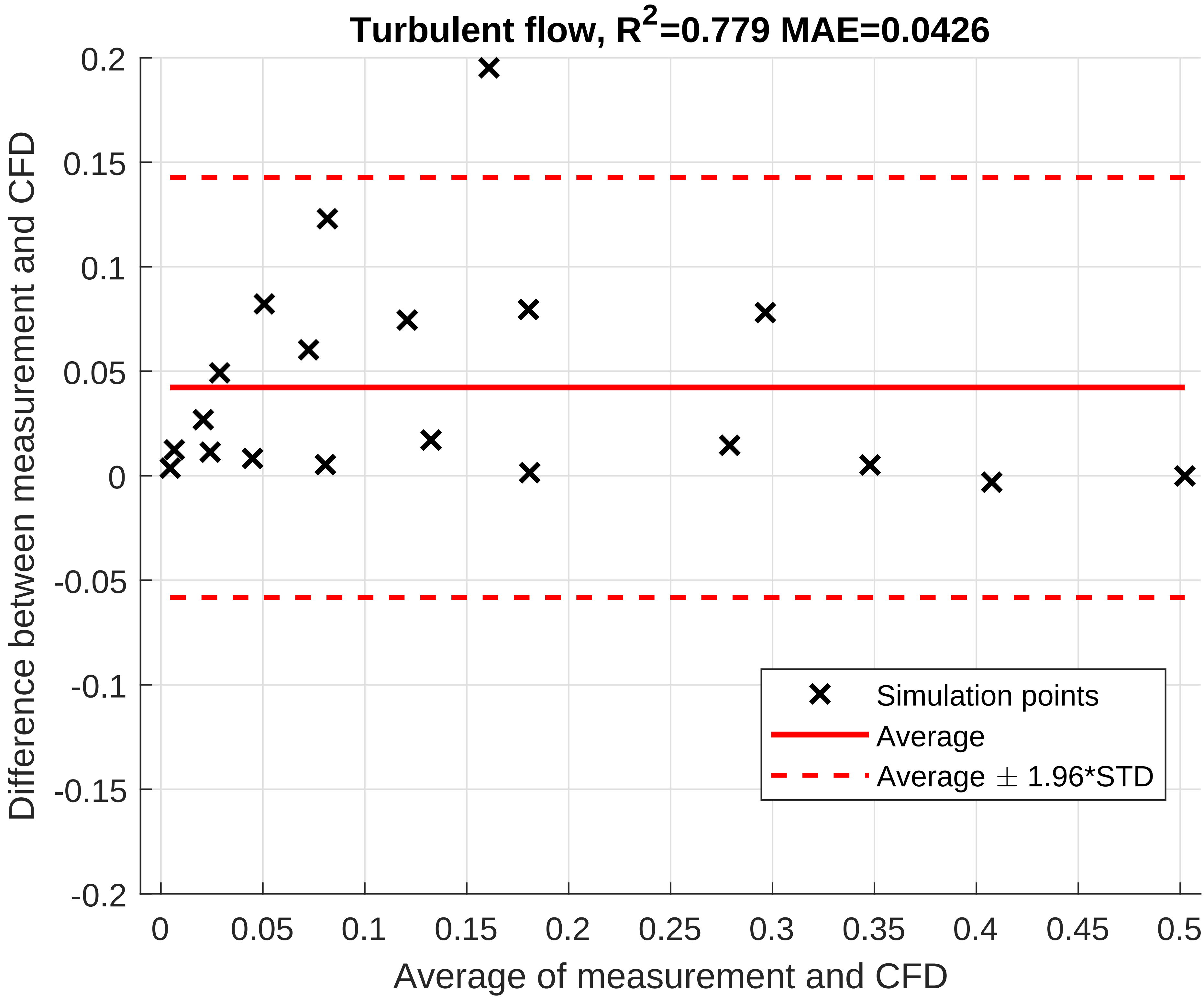
Turbulent flow, R2=0.779 MAE=0.0426
Difference between measurement and CFD
Average of measurement and CFD
0.2
0.15
0.1
0.05
0
-0.05
-0.1
-0.15
-0.2
0
0.05
0.1
0.15
0.2
0.25
0.3
0.35
0.4
0.45
0.5
Simulation points
Average
Average ± 1.96*STD

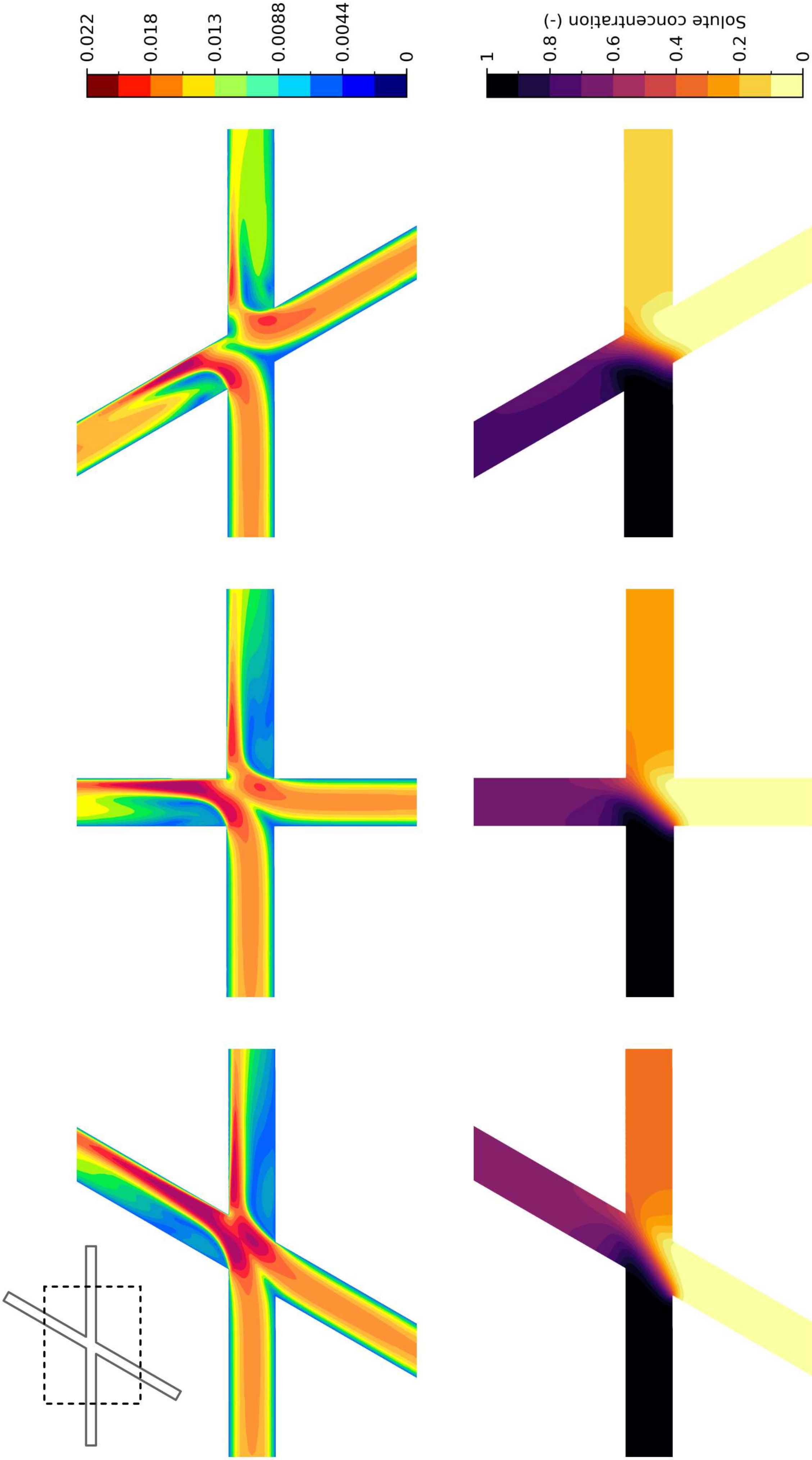
Velocity magnitude (m/s)
0.022
0.018
0.013
0.0088
0.0044
0
Solute concentration (-)
1
0.8
0.6
0.4
0.2
0

Click here to access/download;Figure;fig5.eps

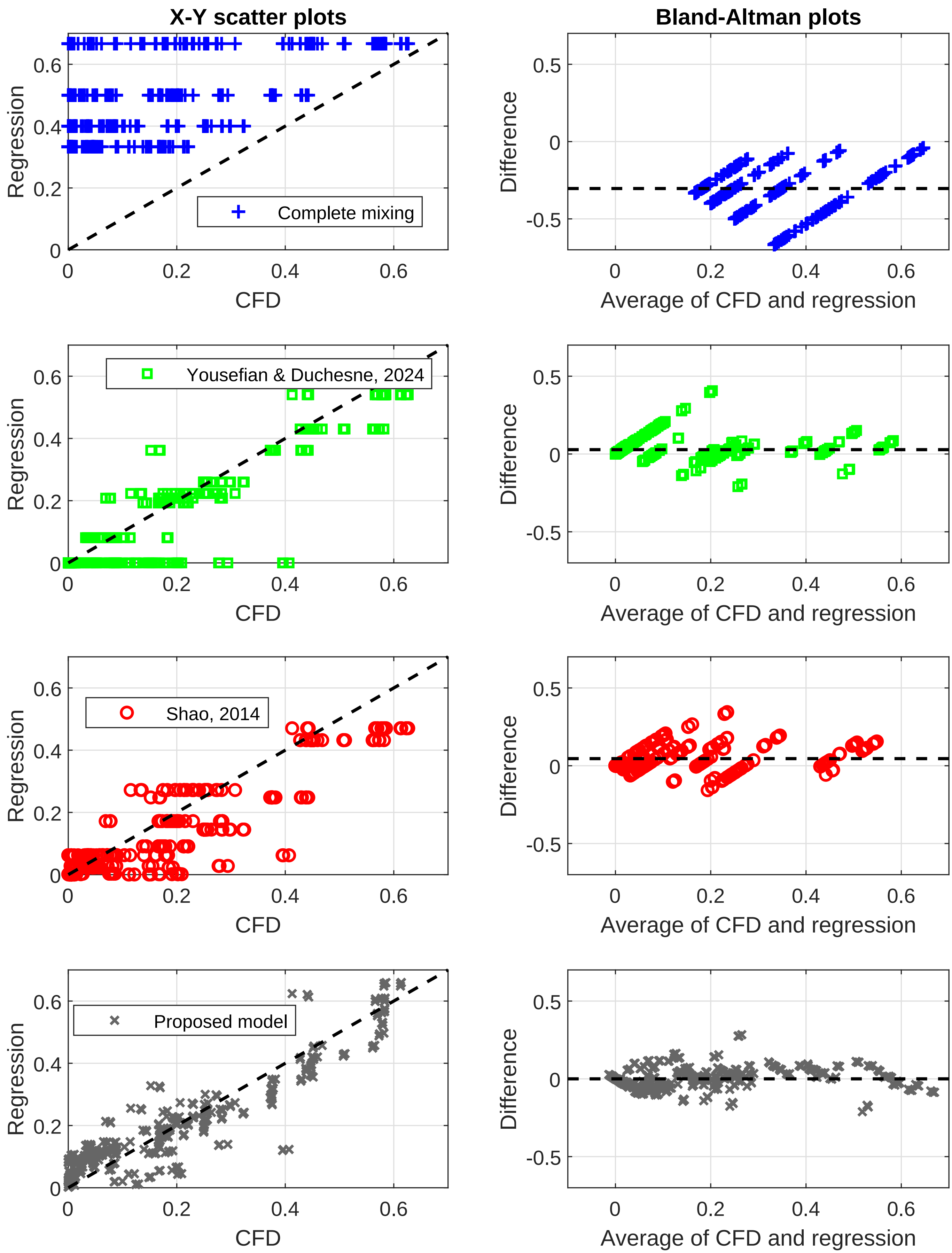

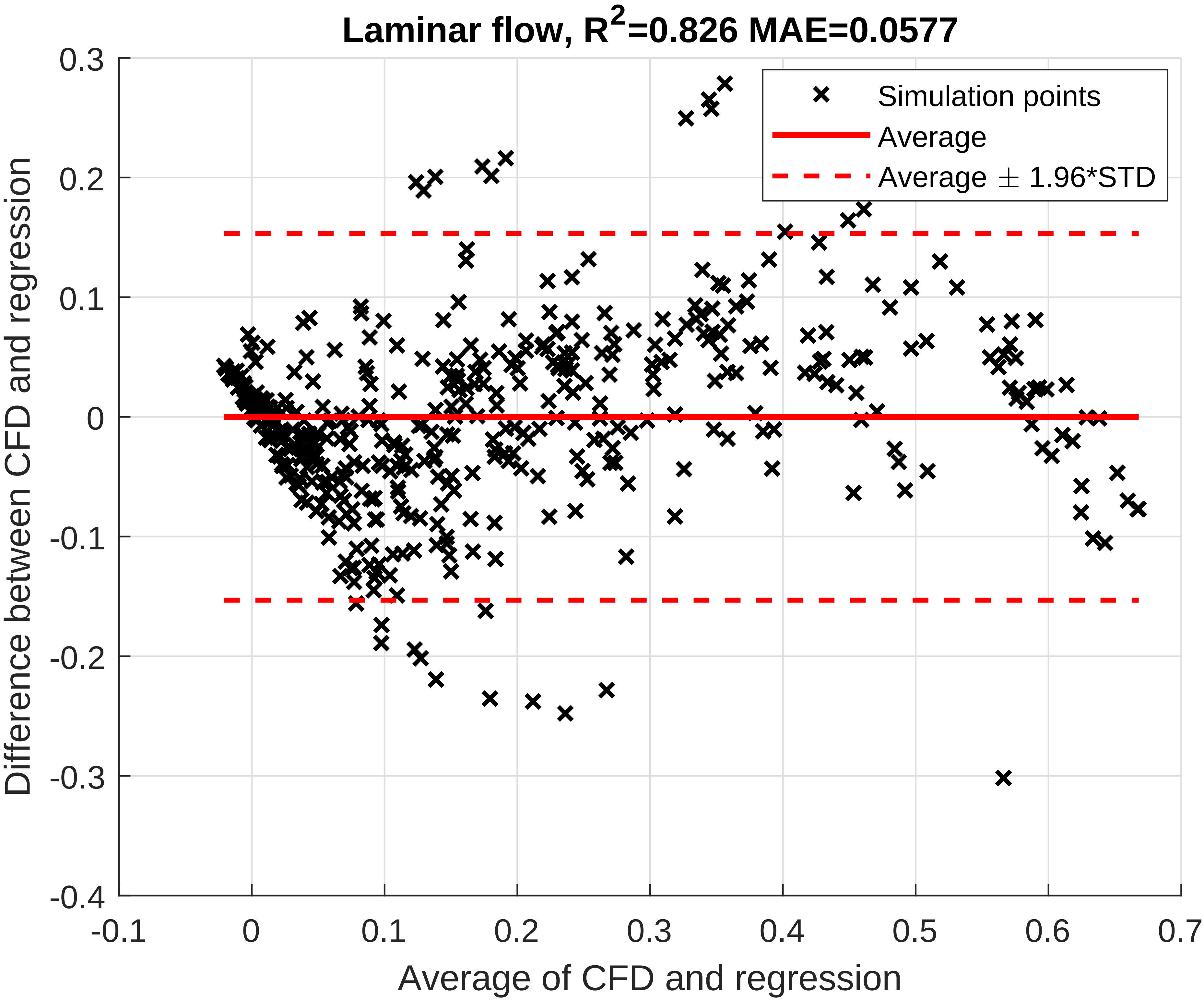
Laminar flow, R^2=0.826 MAE=0.0577
Simulation points
Average
Average ± 1.96*STD
Difference between CFD and regression
Average of CFD and regression
0.3
0.2
0.1
0
-0.1
-0.2
-0.3
-0.4
-0.1
0
0.1
0.2
0.3
0.4
0.5
0.6
0.7

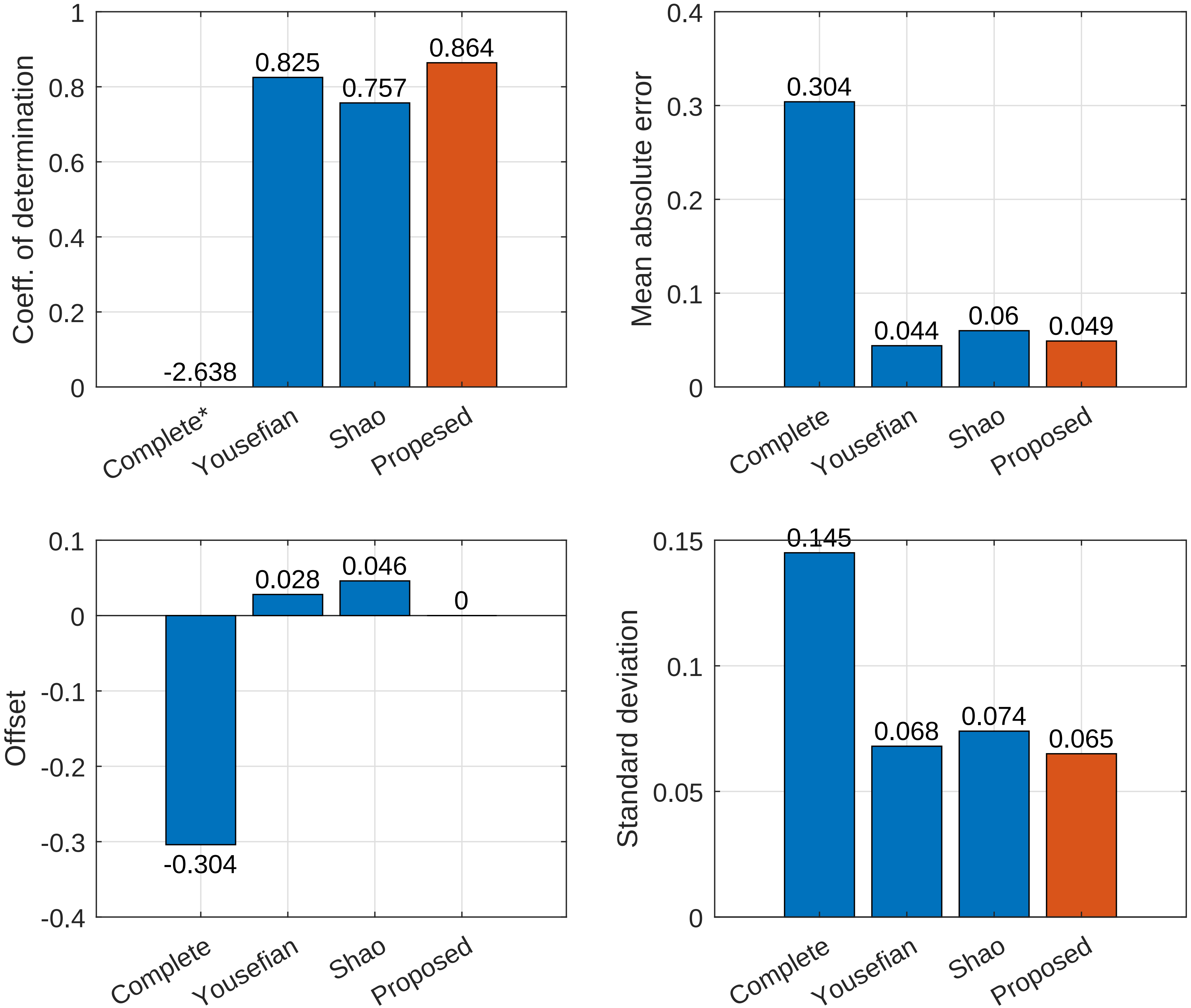
Coeff. of determination
1
0.8
0.6
0.4
0.2
0
-2.638
0.825
0.757
0.864
Complete*
Yousefian
Shao
Propesed
Mean absolute error
0.4
0.3
0.2
0.1
0
0.304
0.044
0.06
0.049
Complete
Yousefian
Shao
Proposed
Offset
0.1
0
-0.1
-0.2
-0.3
-0.4
-0.304
0.028
0.046
0
Complete
Yousefian
Shao
Proposed
Standard deviation
0.15
0.1
0.05
0
0.145
0.068
0.074
0.065
Complete
Yousefian
Shao
Proposed

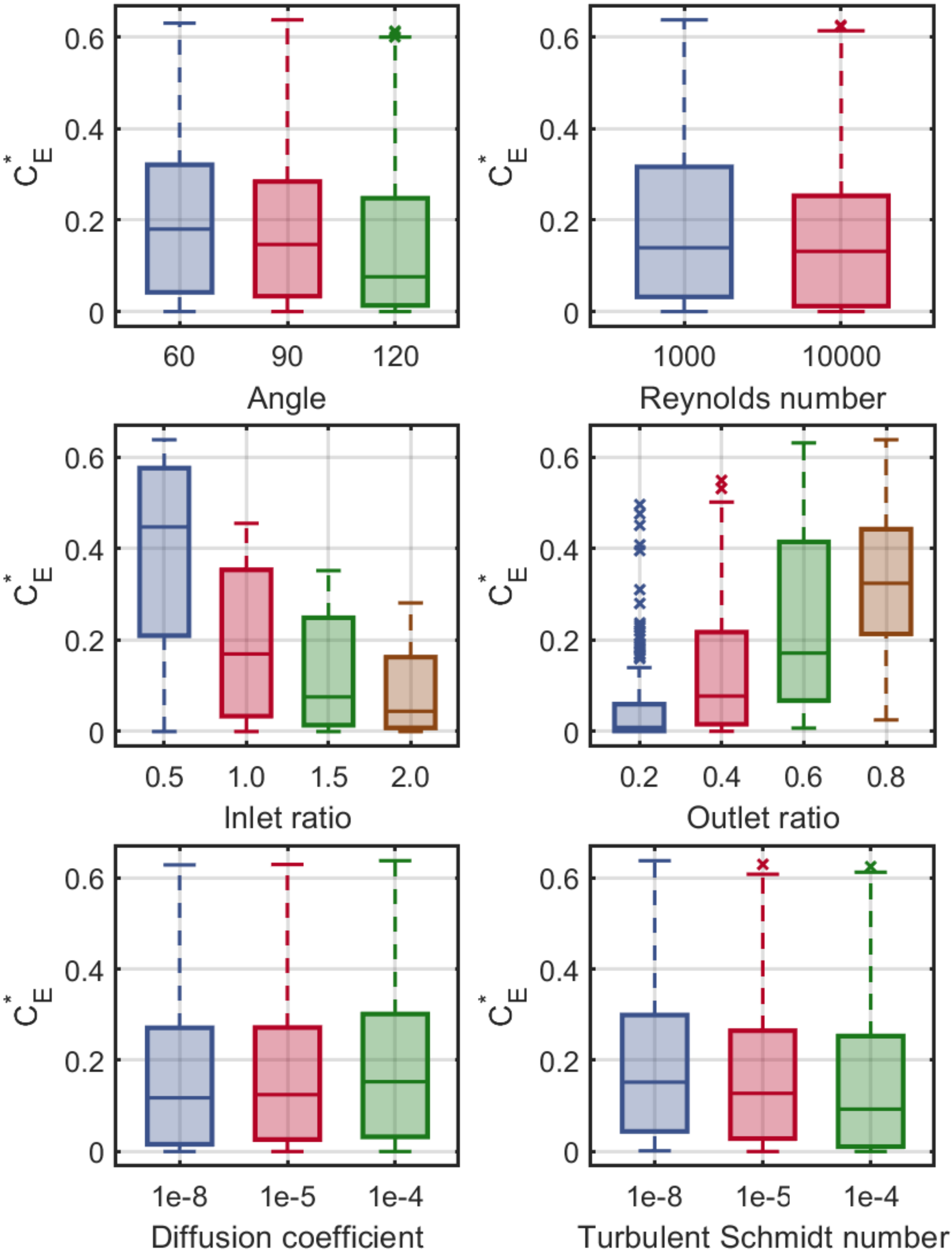

0.6
0.4
0.2
0
C_E^*
60
90
120
Angle
1000
10000
Reynolds number
0.5
1.0
1.5
2.0
Inlet ratio
0.2
0.4
0.6
0.8
Outlet ratio
1e-8
1e-5
1e-4
Diffusion coefficient
Turbulent Schmidt number

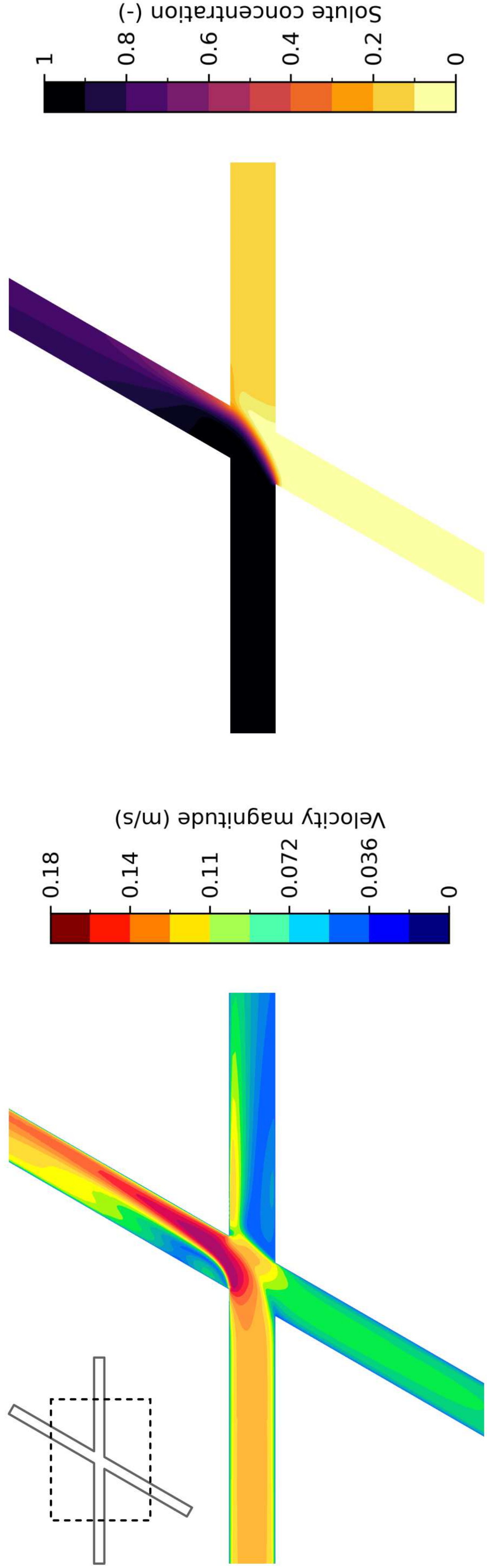
Solute concentration (-)
1
0.8
0.6
0.4
0.2
0
Velocity magnitude (m/s)
0.18
0.14
0.11
0.072
0.036
0

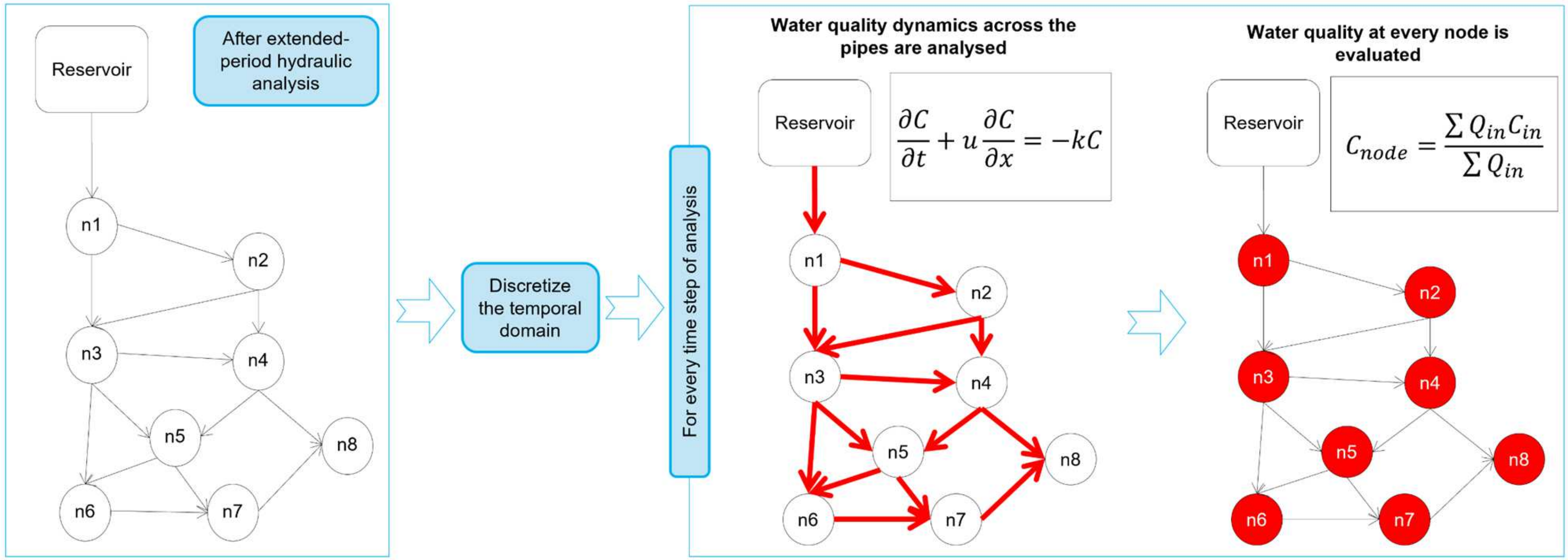

After extended-period hydraulic analysis
Reservoir
n1
n2
n3
n4
n5
n6
n7
n8
Discretize the temporal domain
For every time step of analysis
Water quality dynamics across the pipes are analysed
$\frac{\partial C}{\partial t} + u\frac{\partial C}{\partial x} = -kC$
Water quality at every node is evaluated
$C_{node} = \frac{\sum Q_{in} C_{in}}{\sum Q_{in}}$

(A)

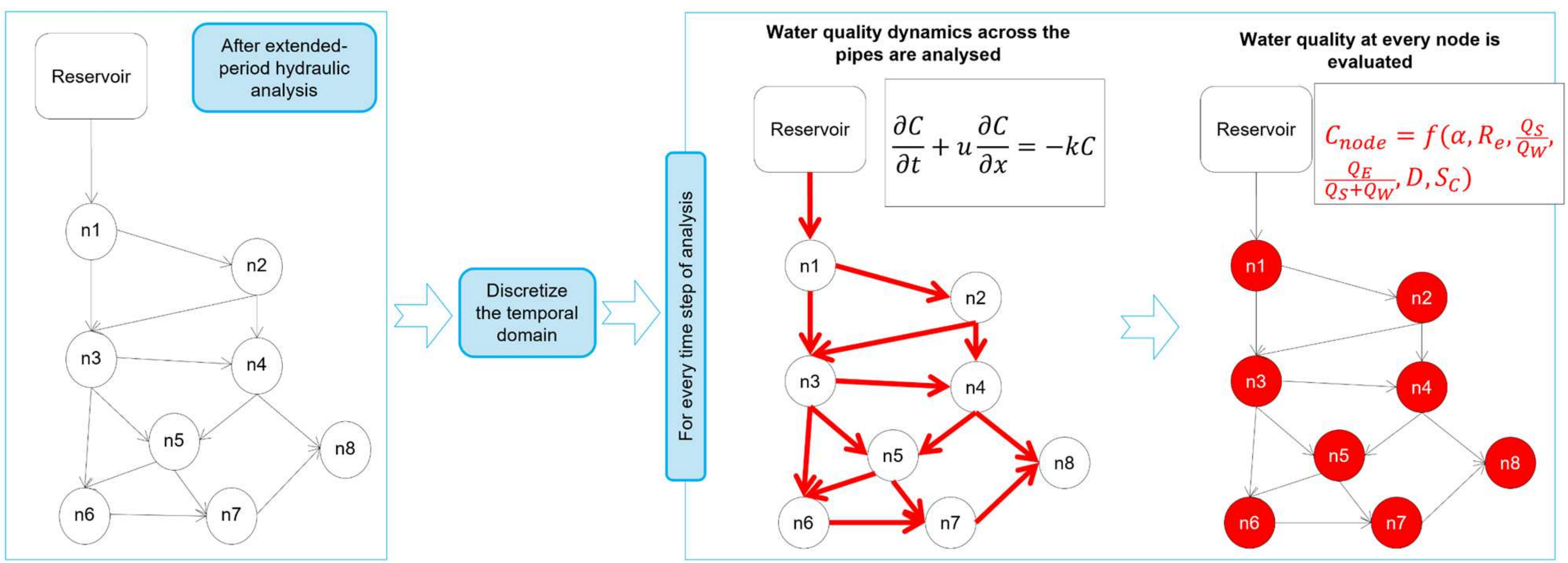

After extended-period hydraulic analysis
Reservoir
n1
n2
n3
n4
n5
n6
n7
n8
Discretize the temporal domain
For every time step of analysis
Water quality dynamics across the pipes are analysed
$\frac{\partial C}{\partial t} + u\frac{\partial C}{\partial x} = -kC$
Water quality at every node is evaluated
$C_{node} = f(\alpha, R_e, \frac{Q_S}{Q_W}, \frac{Q_E}{Q_S+Q_W}, D, S_C)$

(B)

CFD analysis of solute mixing in water distribution network cross-junctions highlights the influence of pipe connection angles and inflow–outflow ratios on incomplete mixing. Regression models capture nonlinear relationships between dominant hydraulic parameters, enabling prediction for integration into WDN solvers such as EPANET.

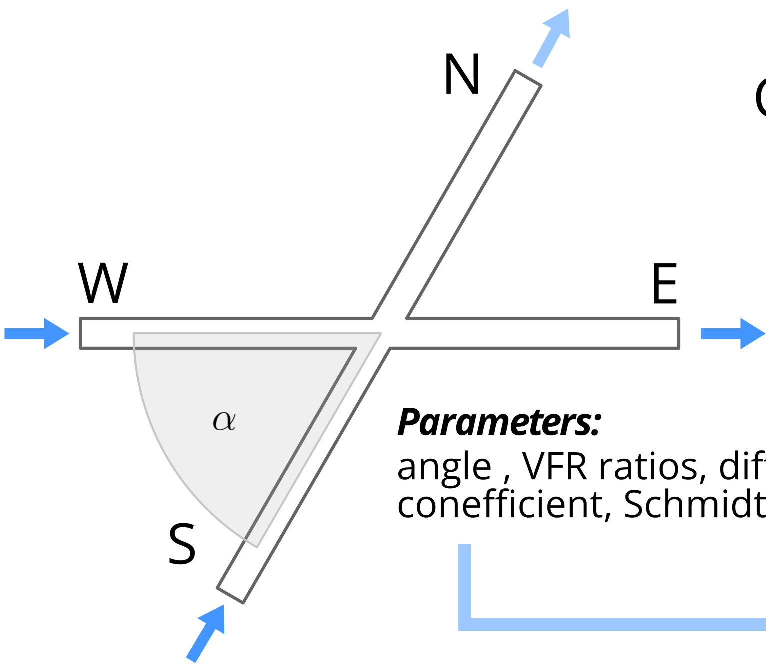

Computational Fluid Dynamics

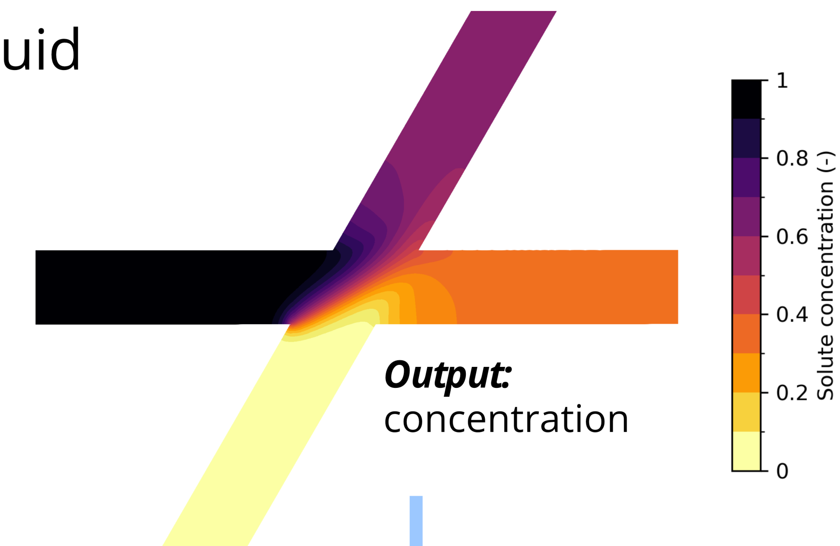

Parameters:
angle , VFR ratios, diffusive coneefficient, Schmidt number

Output:
concentration

Regression model for outlet concentration

$$C_E^* = \beta_1 \left(\log\left(\frac{Q_E}{Q_S}\right) + \beta_2 \left(\frac{Q_W}{Q_E}\right)^{\beta_3} \right) \alpha^{\beta_4} D^{\beta_5} Sc^{\beta_6} + \beta_7$$